IEEE Photonics Journal
An IEEE Photonics Society Publication

Open Access

L_n Slot Photonic Crystal Microcavity for Refractive Index Gas Sensing

Volume 6, Number 5, October 2014

Kezheng Li
Juntao Li
Yanjun Song
Guisheng Fang
Chao Li
Ziying Feng
Rongbin Su
Biaohua Zeng
Xuehua Wang
Chongjun Jin

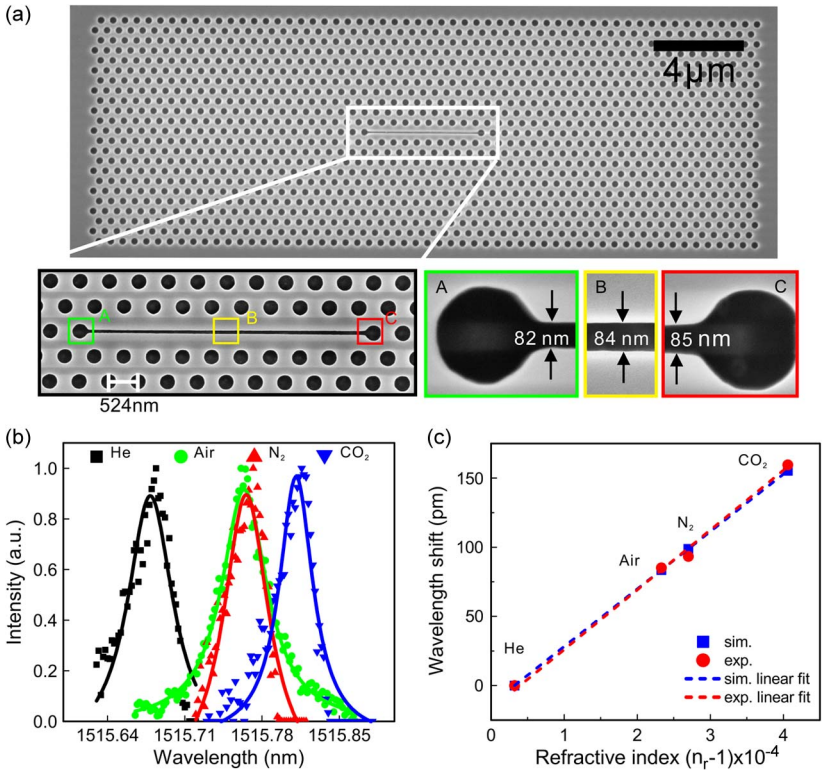

DOI: 10.1109/JPHOT.2014.2360286
1943-0655 © 2014 IEEE

IEEE photonics SOCIETY

IEEE

L_n Slot Photonic Crystal Microcavity for Refractive Index Gas Sensing

Kezheng Li, Juntao Li, Yanjun Song, Guisheng Fang, Chao Li, Ziying Feng, Rongbin Su, Biaohua Zeng, Xuehua Wang, and Chongjun Jin

State Key Laboratory of Optoelectronic Materials and Technologies, School of Physics and Engineering, Sun Yat-sen University, Guangzhou 510275, China

DOI: 10.1109/JPHOT.2014.2360286

Manuscript received August 12, 2014; revised September 11, 2014; accepted September 11, 2014. Date of publication September 25, 2014; date of current version October 1, 2014. This work was supported in part by the National Natural Science Foundation of China under Grant 11174374, Grant 11204386, Grant 11374376, and Grant 11411130117; by the Guangdong Natural Science Foundation under Grant S2012040007812; by the Key project of DEGP under Grant 2012CXZD0001; and by the Chinese National Key Basic Research Special Fund under Grant 2010CB923201. The work of C. Li was supported by the China Postdoctoral Science Foundation under Grant 2013M542222. K. Li and J. Li contributed equally to this work. Corresponding author: C. Jin (e-mail: jinchjun@mail.sysu.edu.cn).

Abstract: We propose and experimentally demonstrate a series of L_n slot photonic crystal (PhC) microcavities, which operate as refractive index (RI) gas sensors. The cavities are simply composed of a silicon slab triangular photonic crystal with n holes replaced by a slot, which do not require sophisticated design or high fabrication resolution. With the increase in n, the quality factor of the cavity exponentially increases, which is explained by the envelope of electric field approaching a Gaussian profile. An L_9 slot PhC microcavity with a quality factor exceeding 30 000, sensitivity of 421 nm per RI unit (RIU), and detection limit down to 1×10^{-5} RIU was experimentally demonstrated. The performance of the device is comparable with other fine-tuned PhC microcavity structures. Due to its simple structure and high fabrication tolerance, it could have wide applications in optical sensors.

Index Terms: Photonic crystals, sensors, microcavity devices.

1. Introduction

Photonic crystal (PhC) microcavities have wide applications in various fields, such as lasers [1], [2], optical switching [3], [4], cavity quantum electrodynamics [5], and bio-chemical sensing [6]–[9], due to their strong field confinement, high quality factors (Q) and small modal volumes. When an air slot is introduced into the PhC microcavity, the electric field discontinuity at the interface with large refractive index (RI) contrast enables higher optical confinement inside the area of low refractive index material [10]. This property enhances the light-matter interaction and results in a high sensitivity towards the local change of the environment. Through the resonant wavelength shift induced by the change of the RI in the slot, high Q PhC microcavities are widely utilized as chemical and biological sensors to detect gases [11], [12], solutions [13]–[17], and bio-molecules [18]. Compared to other types of RI sensors, such as multiple optical mode waveguides [19], Mach-Zehnder interferometers [20] and Young Interferometers [21], slot PhC bio-chemical sensors have advantages of small size, high sensitivity, and CMOS compatibility.

TABLE 1

Summary of different PhC sensors

Structure type	Sensing materials	Q	Sensitivity (nm/RIU)	DL (nm/RIU)
Heterostructure cavity [11]	gas	4.0×10^{4}	80	1.0×10^{-4}
Heterostructure slot cavity [12]	gas	2.6×10^{4}	510	1.0×10^{-5}
Heterostructure slot cavity [14]	liquid	4.0×10^{3}	1538	7.8×10^{-6}
Modified H_1 cavity [13]	liquid	4.0×10^{2}	155	1.8×10^{-2}
Modified L_3 cavity [13]	liquid	2.7×10^{3}	63	6.0×10^{-3}
Modified L_3 cavity [15]	liquid	6.0×10^{3}	98	2.5×10^{-3}
Modified slot cavity [16]	liquid	7.0×10^{3}	370	2.3×10^{-5}
Modified L_7 cavity [17]	liquid	2.6×10^{3}	460	2.7×10^{-4}
L_9 slot microcavity (sim.)	gas	1.28×10^{5}	417	3.3×10^{-6}
L_9 slot microcavity (exp.)	gas	3.29×10^{4}	421	1.0×10^{-5}

For bio-chemical sensing, sensitivity and detection limit (DL) are two important parameters for evaluating sensing abilities. Sensitivity is defined as the ratio between the shift of resonant wavelength and the change of local RI and expressed as [22]

$$S = \frac{\Delta\lambda_r}{\Delta n} = \frac{\Gamma\lambda_r}{n_{eff}} \tag{1}$$

where S is the sensitivity, Γ is the spatial overlap factor between the cavity mode and the analyte, λ_r is the cavity resonant wavelength, and n_{eff} is the effective RI experienced by the cavity mode. In order to increase sensitivity, an additional air slot is introduced, which not only enlarges Γ, but also decreases n_{eff} [23], [24]. DL characterizes the smallest possible spectral shift that can be accurately measured and is defined as [25]

$$DL = \frac{R}{S} \dot{\propto} \frac{1}{S} \cdot \frac{1}{Q} \tag{2}$$

where R is the sensor resolution, and "$\dot{\propto}$" means "approximately proportional to." Equation (2) indicates that a smaller DL can be obtained by increasing S and Q. Thus, both high S and Q are pursued in designing the cavity. In Table 1 in the next section, we list the S, Q, and DL of some PhC cavities that have been reported in the literature. From the table, the heterostructure cavity [26] has the highest Q among all the PhC structures. However, this kind of cavity needs to be carefully optimized and finely tuned in order to achieve ultrahigh Q, and as a result they have a low tolerance to fabrication deviation. For example, the ultimate Q reduces to one eighth of the ideal value when only 1 nm standard deviation is introduced to hole radii [27]. Thus, the fabrication of heterostructure PhC sensors requires sophisticated high resolution, which has limited its development.

In this paper, an L_n $(n > 3)$ microcavity with an air slot, which we refer to as an L_n slot microcavity, was designed and fabricated as a gas sensor. This cavity is simply composed of a slab triangular photonic crystal with n holes in a line replaced by a slot. With the increase of n, the quality factor of the cavity increases exponentially. Importantly, the cavity doesn't require precise nanofabrication technology. Without any geometrical fine tuning, we demonstrate experimentally an L_9 slot microcavity based gas sensor with a $Q \sim 32900$, $S \sim 421$ nm/RIU, and $DL \sim 1 \times 10^{-5}$ RIU, which is the best result for a non-heterostructure PhC sensor.

2. Device Design and Analysis

To obtain a high Q slab PhC microcavity, the electric fields of the cavity mode should be gently confined and possess a Gaussian-like envelope [26], [28], which is usually achieved by carefully modifying the microcavity structure [24], [29]. Here, we propose that the electric fields of L_n slot microcavities are naturally asymptotic to the Gaussian-like envelope when n becomes larger.

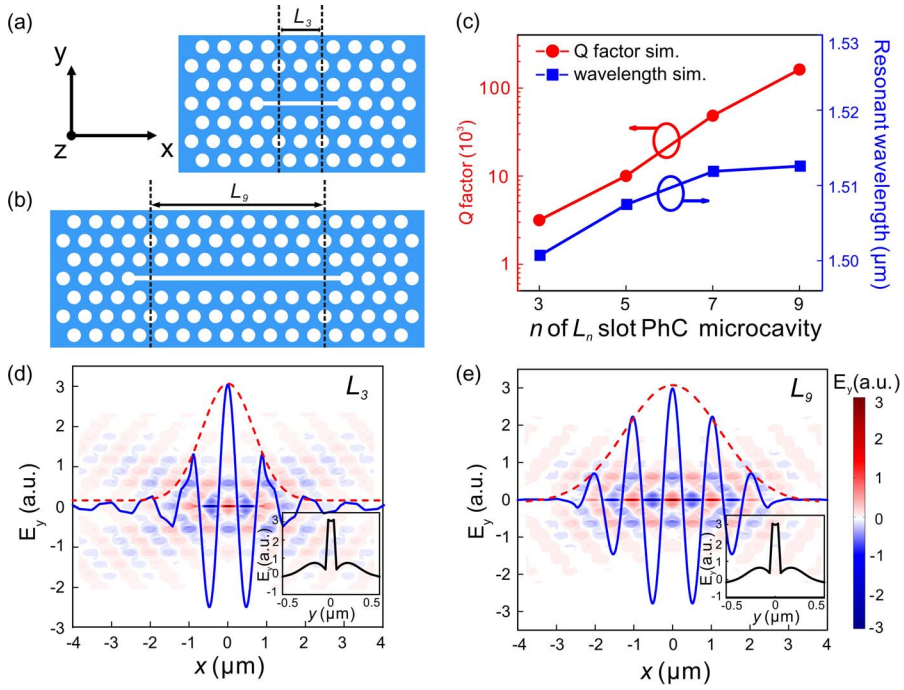

Fig. 1. Schematic sketch of L_n slot cavities. (a) Top view of L_3 slot cavity. (b) Top view of L_9 slot cavity. (c) Dependence of Q and resonant wavelength on the length of the L_n slot cavities. (d) and (e) Electric field distributions of L_3 and L_9 slot cavity where 1-D E_y distributions (blue curve) along the center line of the cavity overlap with 2-D electric field profiles. Red dashed curves represent Gaussian envelopes. Insets are 1-D E_y distributions along the y axis.

A slab PhC with a triangular periodic array of air holes in silicon-on-insulator (SOI) was chosen to build an L_n slot microcavity. The cavity consists of n missing air holes in a line and an air slot links the holes at both ends of the cavity. Fig. 1(a) and (b) are sketches of the L_3 and L_9 slot microcavities. A three-dimensional finite difference time domain method (3D FDTD, RSoft design) was used to evaluate the mode properties. According to the experiment configuration, here we chose the slab RI as 3.4, the slab thickness as 204 nm, the hole radius and slot width as $0.29a$ and $0.16a$ respectively, where $a = 524$ nm is the periodic constant of the PhC. Only TE-like waves are considered here.

The dependence of Q and resonant wavelength on the number n of L_n slot microcavities is shown in Fig. 1(c). The resonant wavelength is slightly red-shift as the cavity length increases. It can be seen that the Q shows an exponential growth with increasing n, where $Q \sim 3 \times 10^3$ for the L_3 slot microcavity, $Q \sim 1 \times 10^4$ for the L_5 slot microcavity, and Q exceeds 10^5 $(\sim 1.3 \times 10^5)$ for the L_9 slot microcavity. This result from the larger L_n slot microcavity presenting a gentler confinement to the electric field, which in turn leads to stronger field localization and smaller energy leakage. This point is also verified by Fig. 1(d) and (e). Compared to the electric field of the L_3 slot microcavity, the field of the L_9 slot microcavity shows a better fit to the Gaussian envelope. The E_y distributions of L_3 and L_9 slot microcavities at the center of the slab are plotted as insets in Fig. 1(d) and (e). The existence of the air slot enhances E_y since the electric displacement D_y is continuous across the slot boundary. As a result, the field can be highly localized in the air region of the slot microcavity, which improves the sensitivity to the change of the environment in the slot. The mode volume (V) of the L_9 slot microcavity is only 0.086 μm^3, and $Q/V \sim 1.6 \times 10^6$ μm^{-3}. For the L_9 slot cavity, the spatial overlap factor is 61.7%. When n changes from 3 to 11, the change of the spatial overlap factor is less than 6%. This means that the performance of the L_n slot cavity is mainly determined by the quality factor according to (2).

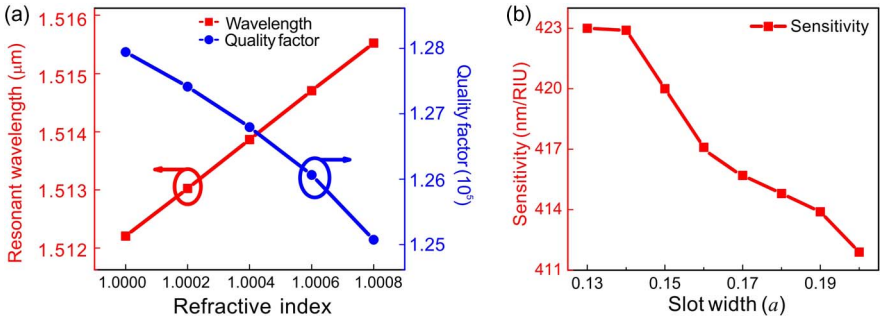

Fig. 2. (a) The variation of resonant wavelength and Q of an L_9 slot cavity with background RI. The slot width is 0.16a. (b) The influence of slot width on sensitivity of the L_9 slot cavity.

Next, we studied the sensing performance of an L_9 slot microcavity. Fig. 2(a) shows the resonant wavelength and Q of the L_9 slot microcavity under different gas background when the slot width is 0.16a. The resonant wavelength has a linear red-shift as the gas RI varies from 1.0 to 1.0008, while the Q decreases a little. The sensitivity is 417 nm/RIU according to (1). It is worth mentioning that $n > 9$ makes no significant difference to the sensitivity, i.e., the simulated sensitivity of an L_{13} slot microcavity is 423 nm/RIU, because the spatial overlap factor is nearly the same.

Fig. 2(b) illustrates the relationship between sensitivity and slot width. As the slot width increases, the resonant wavelength blue shifts and the sensitivity decreases slightly because the effective RI reduces and the cavity mode moves toward the air band. The structure also exhibits a high fabrication tolerance since the sensitivity only fluctuates $\pm 1.7\%$ when the slot width varies from 0.13a to 0.2a (68 nm to 105 nm). Moreover, according to (2), the DL of the cavity is as low as 3.3×10^{-6} RIU, when we take 34.9 dB for the signal to noise ratio (SNR) and 1 pm for the spectrum resolution. The experimental DL is estimated to be 1.0×10^{-5} RIU (see the Experiment section). Therefore, the L_9 slot microcavity possesses high resolution, high sensitivity and low DL compared to other finely tuned PhC sensors (see Table 1). This is the best reported performance for a non-heterostructure PhC sensor. A higher Q and smaller DL can be obtained by further increasing n, but this will also increase the divergence angle slightly and make the cavity more fragile.

3. Fabrication and Optical Characterization of the Device

L_n slot microcavities were fabricated on a silicon-on-insulator wafer (SOITEC Inc.). The top silicon layer is 220 nm. Electron beam lithography (Vistec EBPG 5000 plus) was applied to define the patterns on ZEP-520A positive-tone electron-beam resist with 100 pA writing current and 320 μC/cm^2 expose dose at 100 keV. Then, inductively coupled plasma etching (Oxford PlasmaLab System 180) was used to transfer the patterns from the ZEP resist to the silicon layer with a gas combination (12:15) of SF_6 and C_4F_8 at 4 mTorr and 5 °C. Finally, the 2 μm thick buried oxide (BOX) layer was removed in hydrofluoric acid solution (20%) for 8 minutes to achieve a freestanding silicon membrane structure. A scanning electron microscope (SEM) image of the final structure is shown in Fig. 3(a). The distribution of air hole radii can be described by a Gaussian distribution with mean value being 150 nm and standard deviation of 2 nm, as shown in Fig. 3(b). The periodic constant is 524 nm. Fig. 3(a) shows the mean value of the slot width is 84 nm, or 0.16a.

The performance of an L_n slot microcavity as a RI sensor was characterized by measuring continuous-wave light scattering under various gas atmospheres. The measurement system was based on the method of crossed-polarized resonant scattering [30], as shown in Fig. 3(c) and (d). The sample was mounted in a gas cell with a quartz window. The sample's axis was orientated to the bisector of the angle formed by a polarizer and analyzer to obtain the maximum coupling effect. A tunable continuous wavelength laser ranging from 1495 nm to 1620 nm, with

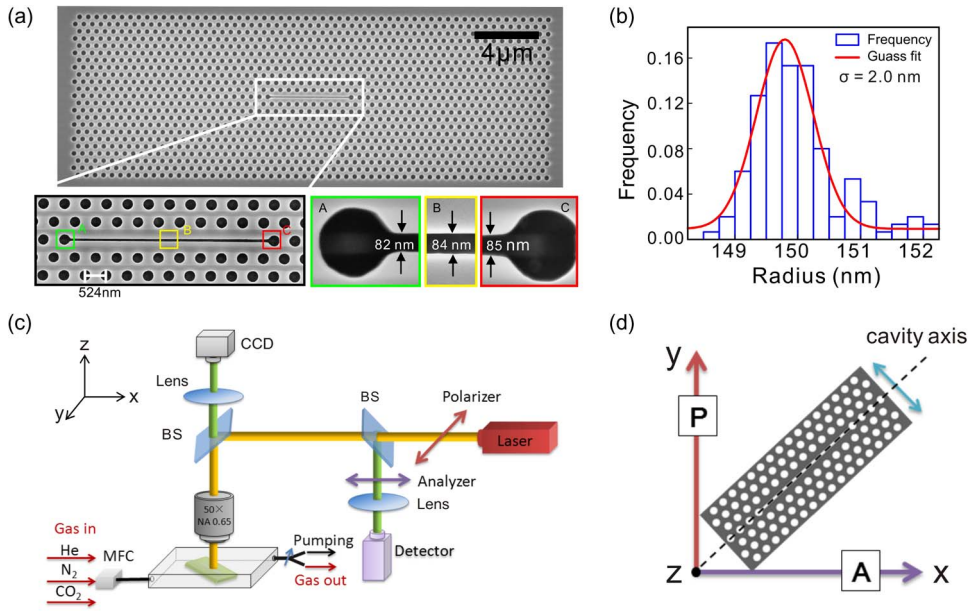

Fig. 3. (a) SEM image of an L_9 slot cavity. A magnified view of the slot cavity is in the left lower panel; zoomed views of regions A, B, and C are shown in the right lower panel. (b) The statistical distribution of the air hole radii and a Gaussian distribution with standard deviation of 2.0 nm (red line). (c) Schematic of the optical detection setup for continuous wavelength laser measurement in crossed polarization. A and P refer to analyzer and polarizer, respectively. (d) The microcavity is mounted so that its axis is oriented to the bisector formed by polarizer and analyzer to obtain the maximum coupling effect. The blue arrow indicates the TE-like cavity mode.

resolution of 1 pm (Santec, TSL 510), was focused on the sample by a NA = 0.65 IR objective lens (Olympus, LMPLAN IR 50×). The backward scattered light from the sample was collected by a beam splitter and analyzed by the analyzer in crossed polarization. The signal was finally detected by a power meter (Yokogawa, AQ 2200-231). The working principle is that only the incoming frequency at the resonance of the cavity mode can interact with the *xy*-polarized cavity mode, and produce a *y*-polarized component in the reflected beam, which can pass through the analyzer and be revealed by the detector. The incident light should illuminate the whole cavity to obtain a Lorentzian line shape reflection peak [30]. With the increase of the cavity length *n*, the light spot has to be enlarged, and less light can interact with the cavity, therefore, the signal to noise ratio (SNR) is decreased rapidly. Taking full consideration of the SNR and *DL*, we found that when $n = 9$, we can get the best results in our experiment. Therefore, we use the L_9 slot cavity as the basic geometry for gas sensing. The *Q* of the sample was obtained by fitting the reflection peak, as shown in Fig. 4.

Fig. 4(a) shows the measured *Q* and resonant wavelength for different L_n slot microcavities. The results are in good agreement with simulation. For the L_3 slot microcavity, the measured *Q* is 2530 while the simulated one is 3160; for the L_9 slot PhC microcavity, the *Q* is 1.28×10^5 in simulation and 3.0×10^4 in experiment. That the measured *Q* is smaller than the simulated one is attributed to disorder-induced scattering loss [31], and surface water absorption loss [32]. The reflection spectrum in Fig. 4(b) shows two well-separated resonant modes. The one with the higher *Q* is used for gas sensing.

During the test, the sample was exposed to different gases, such as nitrogen (N_2, RI $\sim$ 1.000274), helium (He, RI $\sim$ 1.000036), carbon dioxide (CO_2, RI $\sim$ 1.000411), and air (RI $\sim$ 1.000269) [12]. The RI values were recalculated for $\lambda = 1515$ nm at atmospheric pressure and room temperature 20 °C using the ideal gas model [33]. The flow rate of gases was set to 2 sccm by a digital gas mass flow controller (Sevenstar, Inc., MFC CS-200). Before testing, the gas cell was pumped to vacuum to ensure gas purity and avoid the influence of humidity.

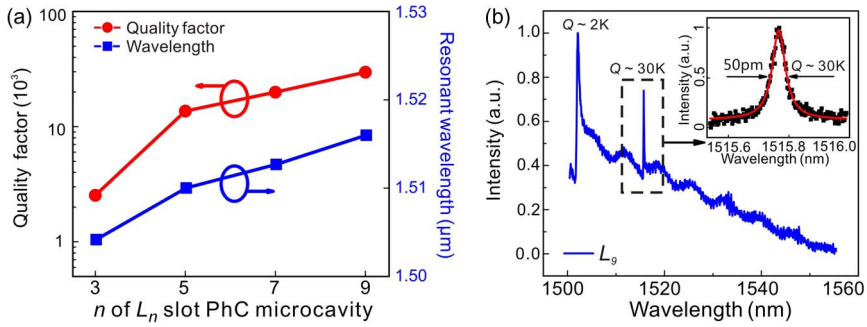

Fig. 4. (a) The dependence of Q and resonant wavelength on the length of the cavity. (b) Reflection spectrum of L_9 slot PhC microcavity. Inset is the normalized Lorentzian fit (red curve) of the resonance.

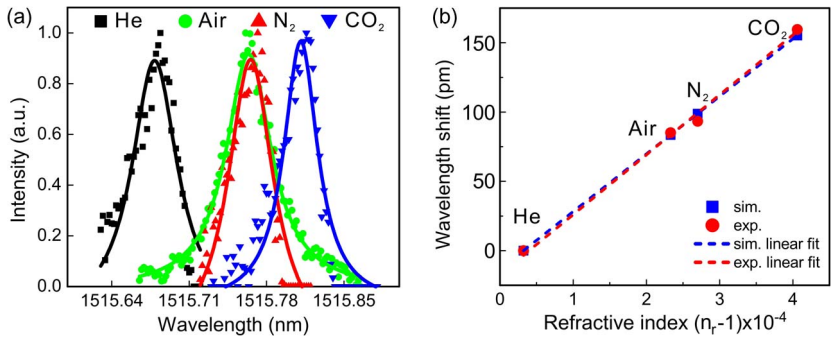

Fig. 5. Experimental results of the L_9 slot microcavity as a gas sensor. (a) Reflection spectra (solid dots) for different gas backgrounds (He, Air, N_2, CO_2). The solid lines represent the corresponding Lorentzian fits. (b) The relationship between the resonant wavelength shift and gas RI. The resonance wavelength for He is used as a reference. The experimental sensitivity is 421 nm/RIU, which is determined by a linear fit (red dashed line). The standard deviations of resonant wavelengths for He, Air, N_2, and CO_2 are 0.0014, 0.0012, 0.0014, and 0.0011 nm, respectively.

Moreover, the measurement—was conducted in the shortest possible time to minimize resonance shift due to progressive oxidation [12]. For accuracy and repeatability, each measurement was repeated five times.

The experimental results of the L_9 slot microcavity are presented in Fig. 5 and Table 1. Fig. 5(a) shows the reflection spectra of the cavity exposed in He, air, N_2 and CO_2 respectively. The average Q is 3.29×10^4. Fig. 5(b) illustrates the simulated and experimental relationship between the resonant wavelength shifts and the gas RI, where the simulated and experimental results agree very well. The sensitivity is 417 nm/RIU in simulation and 421 nm/RIU in experiment. Using the definition in Ref. [25], with signal to noise ratio (SNR) of 34.9 dB under 0.063 mW excitation power, the detection limit of this device is estimated to be 1.0×10^{-5} RIU. Compared to other results listed in Table 1, the L_n slot microcavity sensor is one of the best sensors. We also note that the L_n microcavity sensor has a high tolerance to fabrication defects, originating from the fact that the microcavity with high Q is not dependent on fine geometrical tunings. In all of the experiments, a 2 nm mean deviation is introduced to the hole size. Usually, such a big deviation is not allowed in a fine tuned PhC cavity, and will seriously degrade its Q [17], [27], whereas our experimental Q only dropped to 25% of the simulated value. We discuss the effect of geometrical perturbations in more detail in the following section.

4. Discussion

For the sake of brevity, we focus on an L_9 slot microcavity with a slot width of 84 nm according to the experiment. The structure parameters are perturbed by a random deviation and

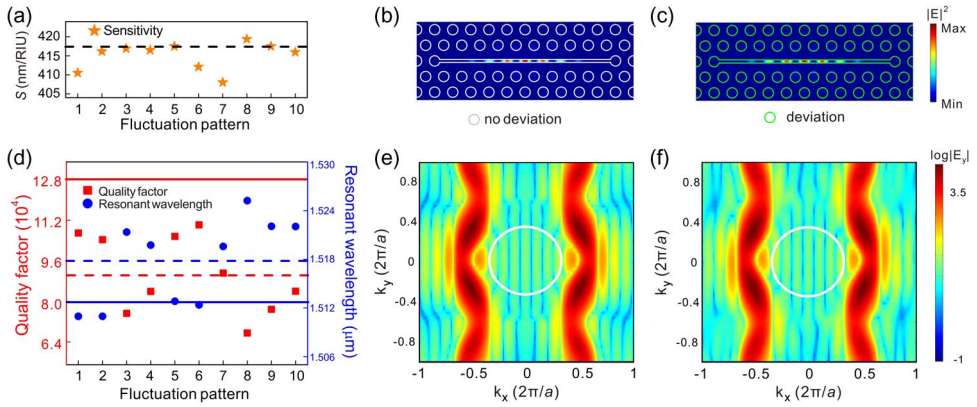

Fig. 6. The effect of deviation of air hole radius, position, and slot width of L_9 slot microcavity. (a) The fluctuation of S with the maximum deviation of $A = 2.5$ nm. The black dashed line represents sensitivity without deviation. (b) and (c) The squared electric field distributions $|E|^2$ on the slab surface representing the nanocavity modes without deviation and with deviation, respectively. (d) The corresponding fluctuation of Q and resonant wavelength. The red and blue dashed lines indicate the average quality factors and resonant wavelengths, respectively. The red and blue solid lines represent the value of quality factor and resonant wavelength without deviation. (e) and (f) The Fourier transform of E_y without deviation and with deviation, respectively. The white circles represent the light cone.

expressed as $M = M_0 + A\delta$ [27], where M_0 is the ideal value of air hole radii or position or slot width, A is the maximum deviation, δ is a random value varying between -1 to 1. In [27], [34], A is about 1 nm from the statistical study of SEM, while the standard deviations of air hole radii and slot width in this paper are about 2.0 nm. Since the positions of the air holes are hard to determine accurately [34], we assume the maximum deviation of positions to be the same as the maximum deviation of radii, namely 2.0 nm. To make our simulation results more reasonable, here we choose $A = 2.5$ nm for all the deviations mentioned above. Fig. 6(a) and (d) represent 10 different random results. The standard resonant wavelength (the blue solid line) is 1.512608 μm in Fig. 6(d), while the perturbed ones fluctuate between 1.510980 μm and 1.525236 μm. The average resonant wavelength (the blue dashed line) shifts by 5.1 nm, only 0.34% away from the standard one (the blue solid line). From Fig. 6(a), the sensitivity of the 10 perturbed patterns only fluctuates $\pm$2.1% from the standard one (the black dashed line). So the influence of deviation on sensitivity is quite small.

The squared electric field distributions of the cavity mode without and with perturbation (the 8th fluctuated pattern) are plotted in Fig. 6(b) and (c), respectively. It is clear that in both cases, the majority of the electric-field is localized in the slot region. Considering the electric-field on the slab surface [27], the ratio of squared electric-field in the slot region to the total squared electric-field is 39.6% for the structure without deviation, and 44.3% for the structure with deviation. Fig. 6(e) and (f) show the absolute value of the spatial Fourier transform of E_y on a log scale without and with perturbation. The white circles represent the light cone. We can see that the main field components in k space for the microcavity modes are hardly deformed by the nanometer scale variations. As the fraction of the field in the light cone defines the Q of the microcavity [27], it is obvious that this quantity doesn't change much after perturbation, so the Q of the structure still remains high $(> 6.7 \times 10^4)$. In Fig. 6(d), the average Q of the structures with random deviations is 9.06×10^4 (the red dashed line), approximately 70.6% of the standard one (the red solid line). As the design itself does not contain any sensitive factors which relate to position or size of the holes, the structure retains good performance even after several nanometer fabrication fluctuations. According to coupled mode theory, the measured quality factor Q_{total} is $1/Q_{total} = 1/Q_{int\ rinsic} + 1/Q_{disorder}$ [35], [36], where $Q_{int\ rinsic}$ is the Q in the absence of disorder, and $Q_{disorder}$ is associated with disorder induced losses. Hence, this perturbation will have a dramatic effect if the Q factor is larger than 1 million [36], even though, for the fine tuned L_3 PhC

cavity with medium Q around 10^5, an average Q reduces to 44.6% with the standard deviation of 2.5 nm [36]. Compared to our results, it is obvious that the L_9 slot cavity will still work even if the fabrication isn't perfect.

5. Conclusion

In this paper, we propose a gas sensor based on the L_n $(n > 3)$ slot microcavity. This device possesses both high Q and sensitivity without sophisticated geometrical turning. The high sensitivity is caused by the air slot in the cavity, which enlarges the overlap region between the cavity mode and the gas, while the high Q comes from a relatively large cavity length. Since our design is not based on geometrical tuning, the sensor has a high fabrication tolerance. The sensitivity only fluctuates $\pm 1.7\%$ for different slot widths ranging from 68 nm to 105 nm. We experimentally demonstrated an L_9 slot microcavity with Q exceeding 3.0×10^4, $S \sim 421$ nm/RIU, and $DL \sim 1.0 \times 10^{-5}$ RIU, which is the best result for non-heterostructure PhC sensors. Moreover, the L_9 slot microcavity is not sensitive to geometrical perturbation. Even for perturbations as large as 2.5 nm, the device can still retain high Q (70% of original one) and stable sensitivity (fluctuations within $\pm 2.1\%$ of original one) which is better than other finely designed structures. Due to the small size, high fabrication tolerance, and good sensing characteristics, the L_n slot microcavity has great potential in on-chip sensing.

Acknowledgement

The authors would like to acknowledge T. P. White, E. R. Martins, and W. Whelan-Curtin for useful discussions.

References

[1] K. Hirose *et al.*, "Watt-class high-power, high-beam-quality photonic-crystal lasers," *Nature Photon.*, vol. 8, no. 5, pp. 406–411, Apr. 2014.
[2] Y. Takahashi and S. Noda, "Breakthroughs in photonics 2013: A microwatt-threshold raman silicon laser," *IEEE Photon. J.*, vol. 6, no. 2, art. no. 0700105, Apr. 2014.
[3] K. Nozaki *et al.*, "Ultralow-energy and high-contrast all-optical switch involving Fano resonance based on coupled photonic crystal nanocavities," *Opt. Exp.*, vol. 21, no. 10, pp. 11 877–11 888, May 2013.
[4] K. Nozaki *et al.*, "Sub-femtojoule all-optical switching using a photonic-crystal nanocavity," *Nature Photon.*, vol. 4, no. 7, pp. 477–483, Jul. 2010.
[5] C. J. Hood, M. S. Chapman, T. W. Lynn, and H. J. Kimble, "Real-time cavity QED with single atoms," *Phys. Rev. Lett.* vol. 80, no. 19, pp. 4157–4160, May 1998.
[6] M. G. Scullion, T. F. Krauss, and A. Di Falco, "Slotted photonic crystal sensors," *Sensors*, vol. 13, no. 3, pp. 3675–3710, Mar. 2013.
[7] Y. Zhao, Y. Zhang, and Q. Wang, "Research advances of photonic crystal gas and liquid sensors," *Sen. Actuators B, Chem.*, vol, 160, no. 1, pp. 1288–1297, Dec. 2011.
[8] C. Feng *et al.*, "Design of an ultracompact optical gas sensor based on a photonic crystal nanobeam cavity," *Laser Phys. Lett.*, vol. 9, no. 12, pp. 875–878, Dec. 2012.
[9] Y. Zhang, Y. Zhao, and Q. Wang, "Optimizing the slow light properties of slotted photonic crystal waveguide and its application in a high-sensitivity gas sensing system," *Meas. Sci. Technol.*, vol. 24, no. 10, pp. 105109, Sep. 2013.
[10] J. Robinson, C. Manolatou, L. Chen, and M. Lipson, "Ultrasmall mode volumes in dielectric optical microcavities," *Phys. Rev. Lett.*, vol. 95, no. 14, pp. 143901-1–143901-4, Sep. 2005.
[11] T. Sünner *et al.*, "Photonic crystal cavity based gas sensor," *Appl. Phys. Lett.*, vol. 92, no. 26, pp. 261112, Jul. 2008.
[12] J. Jágerská, H. Zhang, Z. Diao, N. L. Thomas, and R. Houdré, "Refractive index sensing with an air-slot photonic crystal nanocavity," *Opt. Lett.*, vol. 35, no. 15, pp. 2523–2525, Aug. 2010.
[13] D. Dorfner *et al.*, "Silicon photonic crystal nanostructures for refractive index sensing," *Appl. Phys. Lett.* vol. 93, no. 18, pp. 181 103, Nov. 2008.
[14] A. Falco, L. Faolain, and T. Krauss, "Chemical sensing in slotted photonic crystal heterostructure cavities," *Appl. Phys Lett*, vol. 94, no. 6, pp. 063503, Feb. 2009.
[15] C. Kang, C. T. Phare, Y. A. Vlasov, S. Assefa, and S. M. Weiss, "Photonic crystal slab sensor with enhanced surface area," *Opt. Exp.*, vol. 18, no. 26, pp. 27 930–27 937, Dec. 2010.
[16] S. H. Mirsadeghi, E. Schelew, and J. F. Young, "Photonic crystal slot-microcavity circuit implemented in silicon-on-insulator: High Q operation in solvent without undercutting," *Appl. Phys. Lett.*, vol. 102, no. 13, pp. 131115-1–131115-4, Apr. 2013.
[17] Y. Liu and H. Salemink, "Photonic crystal-based all-optical on-chip sensor," *Opt. Exp.*, vol. 20, no. 18, pp. 19 912–19 920, Aug. 2012.

[18] M. Scullion, A. Di Falco, and T. Krauss, "Slotted photonic crystal cavities with integrated microfluidics for biosensing applications," *Biosens. Bioelectron.*, vol. 27, no. 1, pp. 101–105, Sep. 2011.
[19] Z. Yu and S. Fan, "Extraordinarily high spectral sensitivity in refractive index sensors using multiple optical modes," *Opt. Exp.*, vol. 19, no. 11, pp. 10 029–10 040, May 2011.
[20] E. F. Schipper *et al.*, "The realization of an integrated Mach–Zehnder waveguide immunosensor in silicon technology," *Sens. Actuators B, Chem.*, vol. 40, no. 2–3, pp. 147–153, May 1997.
[21] A. Brandenburg and R. Henninger, "Integrated optical Young interferometer," *Appl. Opt.*, vol. 33, no. 25, pp. 5941–5947, Sep. 1994.
[22] N. Mortensen, S. Xiao, and J. Pedersen, "Liquid-infiltrated photonic crystals: Enhanced light-matter interactions for lab-on-a-chip applications," *Microfluidics Nanofluidics*, vol. 4, no. 1–2, pp. 117–127, Jan. 2007.
[23] J. Robinson, C. Manolatou, L. Chen, and M. Lipson, "Ultrasmall mode volumes in dielectric optical microcavities," *Phys. Rev. Lett.*, vol. 95, no. 14, pp. 143901, Sep. 2005.
[24] A. Falco, L. Faolain, and T. Krauss, "Dispersion control and slow light in slotted photonic crystal waveguides," *Appl. Phys. Lett.*, vol. 92, no. 8, pp. 083501, Feb. 2008.
[25] I. White and X. Fan, "On the performance quantification of resonant refractive index sensors," *Opt. Exp.*, vol. 16, no. 2, pp. 1020–1028, Jun. 2008.
[26] B. Song, S. Noda, T. Asano, and Y. Akahane, "Ultra-high-Q photonic double-heterostructure nanocavity," *Nature Mater.*, vol. 4, no. 3, pp. 207–210, Feb. 2005.
[27] H. Hagino, Y. Takahashi, Y. Tanaka, T. Asano, and S. Noda, "Effects of fluctuation in air hole radii and positions on optical characteristics in photonic crystal heterostructure nanocavities," *Phys. Rev. B*, vol. 79, no. 8, pp. 085112-1–085112-8, Feb. 2009.
[28] Y. Akahane, T. Asano, B. S. Song, and S. Noda, "Fine-tuned high-Q photonic-crystal nanocavity," *Opt. Exp.*, vol. 13, no. 4, pp. 1202–1214, Feb. 2005.
[29] T. Asano, B. S. Song, Y. Akahane, and S. Noda, "Ultrahigh-Q nanocavities in two-dimensional photonic crystal slabs," *IEEE J. Sel. Topic Quantum Electron.*, vol. 12, no. 6, art. no. 9233779, pp. 1123–1134, Nov.–Dec. 2006.
[30] M. Galli *et al.*, "Light scattering and Fano resonances in high-Q photonic crystal nanocavities," *Appl. Phys. Lett.*, vol. 94, no. 7, pp. 071101-1–071101-3, Feb. 2009.
[31] E. Kuramochi *et al.*, "Disorder-induced scattering loss of line-defect waveguides in photonic crystal slabs," *Phys. Rev. B.*, vol. 72, no. 16, pp. 161318(R), Oct. 2005.
[32] H. Sekoguchi, Y. Takahashi, T. Asano, and S. Noda, "Photonic crystal nanocavity with a Q-factor of $\sim$9 million," *Opt. Exp.*, vol. 22, no. 1, pp. 916–924, Jan. 2014.
[33] Y. Clergent, C. Durou, and M. Laurens, "Refractive index variations for argon, nitrogen, and carbon dioxide at $\lambda =$ 632.8 nm (He-Ne laser light) in the range 288.15 KT323.15 K, $0 < p <$ 110 kPa," *J. Chem. Eng. Data*, vol. 44, no. 2, pp. 197–199, Jan. 1999.
[34] T. Asano, B. S. Song, and S. Noda, "Analysis of the experimental Q factors ($\sim$1 million) of photonic crystal nanocavities," *Opt. Exp.*, vol. 14, no. 5, pp. 1996–2002, Mar. 2006.
[35] D. Gerace and L. C. Andreani, "Effects of disorder on propagation losses and cavity Q-factors in photonic crystal slabs," *Photon. Nanostruct.*, vol. 3, no. 2–3, pp. 120–128, Dec. 2005.
[36] S. L. Portalupi *et al.*, "Deliberate versus intrinsic disorder in photonic crystal nanocavities investigated by resonant light scattering," *Phys. Rev. B*, vol. 84, no. 4, pp. 045423, Jul. 2011.